MEASUREMENT OF THE SELF-DIFFUSION COEFFICIENT OF WATER AS A FUNCTION OF POSITION IN WHEAT GRAIN USING NUCLEAR MAGNETIC RESONANCE IMAGING

C. D. ECCLES, P. T. CALLAGHAN, AND C. F. JENNER*
Department of Physics and Biophysics, Massey University, Palmerston North, New Zealand; and
*Department of Plant Physiology, Waite Agricultural Research Institute, The University of Adelaide,
Glen Osmond SA 5064, Australia

ABSTRACT   A pulsed field gradient spin echo sequence has been incorporated in a nuclear magnetic resonance (NMR) imaging experiment to provide an image contrast dependent on local molecular self-diffusion. The consequent image attenuation is shown to exhibit a dependence on applied magnetic field gradient consistent with the Stejskal-Tanner relationship. The method used represents a novel extension of microscopic imaging and demonstrates the possibility of measuring localized motion.

Water self-diffusion rates normal to the transverse 1.3-mm section of a wheat grain have been measured in structural features at 150-μm resolution. The results are consistent with averaged measurements in the bulk grain obtained by other methods while local differences in water mobility correlate with differences in physiological function.

INTRODUCTION

The first use of magnetic field gradients to measure nuclear spin densities by nuclear magnetic resonance (NMR) (1, 2) was preceded, two decades earlier, by their use in the measurement of the mean positional changes of nuclei over the time scale of a spin echo experiment (3). In particular the spin echo technique has been used for many years to measure molecular self-diffusion. This method was later refined by Stejskal and Tanner (4) who showed that the imposition of intense pulsed gradients in a spin echo sequence (PGSE) could be used to measure molecular displacements over a well defined time scale. Here we report on an amalgamation of the pulsed gradient spin echo and steady gradient NMR imaging experiment in which localized self-diffusion of water is observed in a sliced section of wheat grain at a transverse resolution of ~150 μm.

Nuclear magnetic resonance imaging employs the spatial dependence of nuclear Larmor frequencies in the presence of applied magnetic field gradients to determine nuclear position. Protons have the greatest Larmor frequency among stable nuclei and therefore provide the greatest sensitivity. In biological tissue, the most abundant source of ^{1}H nuclei is the water molecule and in most cases proton density may be equated with water density in NMR imaging. Proton-containing molecular species may be distinguished by their transverse (T_2) and longitudinal (T_1) relaxation times and differences between the two provide an image contrast mechanism sensitive to molecular dynamics on a local scale. In particular these relaxation times are dependent on the reorientation of internuclear ^{1}H-^{1}H vectors associated with molecular tumbling or segmental motion. For example, the T_2 contrast between water and cellulose protons in plant tissue is so great that the water signal entirely dominates the image.

Recently it has been shown that NMR imaging may be used on a microscopic (submillimeter) scale to image water distribution in plant stems (5). In those systems water transverse relaxation times are typically of order 10 ms in contrast with the 50–100 ms values prevailing in animal tissue (6). This requires an imaging pulse sequence more compact in time than those used in medical imaging in order to minimize the loss of signal resulting from relaxation. Microscopic imaging further differs from its large-scale counterpart in the need for larger magnetic field gradients and in the careful attention that must be given to maximizing signal to noise. It is the loss of signal consequent on reducing the voxel size which ultimately limits the resolution (7) available in a given imaging time. On our system, operating at 60 MHz, we have achieved a voxel resolution of order 100 μm corresponding to a transverse resolution of 30 μm in a slice 1.5-mm thick (imaging time 30 min).

The resolution available is sufficient to reveal major structural features in wheat kernels, for which sufficient longitudinal symmetry exists to justify a slice thickness of order 1 mm. Previous bulk diffusion measurements by

radioactive tracer (Jenner, C. F., and G. P. Jones, manuscript in preparation) and pulsed gradient spin echo (8; Jenner, C. F., and G. P. Jones, manuscript in preparation) methods have shown an average water self-diffusion rate of 6 to 7 $\times$ 10^{-10} m^2 s^{-1} along the grain axis. The present work represents the first attempt to elucidate the dependence of water diffusion on the local structural feature.

THEORY

Combined Dynamic/Static Imaging

Whereas NMR imaging reveals a static spin density $\rho(\mathbf{r})$, the PGSE experiment is sensitive to the probability distribution of displacements by $(\mathbf{r}' - \mathbf{r})$ over a time t. The pulse sequence used in the PGSE experiment is shown in Fig. 1. Because of molecular translation between the first and second gradient pulses, the precessions occurring under the two gradients are imperfectly refocussed leaving a residual phase displacement ϕ_D for each spin. The echo amplitude is given by

$$A(\mathbf{G}) = \overline{\langle J_z (0) \rangle} \exp\left(-\frac{t}{T_2}\right) \overline{\exp [i \, \phi_D \ (\text{echo})]}, \quad (1)$$

where $\langle J_z (0) \rangle$ is the initial longitudinal polarization and $\mathbf{G}$ is the gradient in the longitudinal magnetic field, ∇B_0. The ensemble average of phase displacements is taken at the time of the echo and may be written (10), for nuclei of gyromagnetic ratio γ,

$$\overline{\exp [i \, \phi_D \ (\text{echo})]} = \iiint_V \rho(\mathbf{r}) \iiint_{V'} P_s (\mathbf{r}|\mathbf{r}', t)$$
$$\cdot \exp [-i\gamma\delta (\mathbf{r}' - \mathbf{r}) \cdot \mathbf{G}] \, dV \, dV', \quad (2)$$

where $\rho(\mathbf{r})$ is the (normalized) density of initial spin positions and $P_s (\mathbf{r}|\mathbf{r}', t)$ is the conditional probability that a spin initially at $\mathbf{r}$ has moved to $\mathbf{r}'$ after a time t.

The PGSE experiment of Fig. 1 thus obtains an average of $P_s (\mathbf{r}|\mathbf{r}', t)$ over the nuclear population. In a homogeneous sample the average involves no loss of information and Eq. 2 reveals many useful features. For example, where no net displacement occurs, $\overline{(\mathbf{r}' - \mathbf{r})} = 0$. In this case the mean echo phase factor, $\overline{\exp [i \, \phi_D \ (\text{echo})]}$ will be real with the echo signal entirely "in phase" but with its amplitude attenuated. The presence of net phase shifts may in fact be
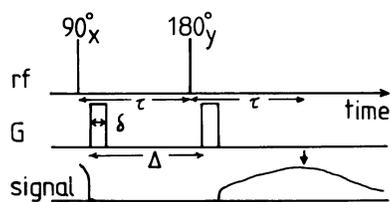
FIGURE 1 Pulsed gradient spin echo sequence used to measure molecular displacement over the timescale Δ. The choice of applied gradient direction determines the component of displacement to which the image amplitude is sensitive.

used as a signature for flow. The dependence of Eq. 2 on δ, t, and G yields $P_s(\mathbf{r}|\mathbf{r}', t)$ in detail. We shall be concerned with the simple case of self-diffusion for which

$$P_s = (\pi \, \sigma^2)^{-3/2} \exp [- (\mathbf{r}' - \mathbf{r})^2 /2\sigma^2]$$
$$\sigma^2 = 2Dt, \quad (3)$$

where D is the molecular self-diffusion coefficient.

As shown by Stejskal and Tanner (4), for gradient pulses of finite duration δ and separation Δ,

$$\overline{\exp [i \, \phi_D \ (\text{echo})]} = \exp [-\gamma^2 \, \delta^2 \, G_z^2 D(\Delta - \frac{1}{3} \delta)], \quad (4)$$

where in this example the self-diffusion is measured along the z-axis, the direction of the pulsed gradient of magnitude G_z. In disperse samples the averaging over $\rho(\mathbf{r})$ masks the dependence of $P_s(\mathbf{r}|\mathbf{r}', t)$ on $\mathbf{r}$. For example, where self-diffusion differs from place to place in the sample, the basic PGSE experiment yields only an appropriately weighted average of echo attenuations. $\rho(\mathbf{r})$ is of course the static spin distribution obtained in NMR imaging and by combining the PGSE and imaging sequence, as shown in Fig. 2, the separation of $\rho(\mathbf{r})$ and $P_s(\mathbf{r}|\mathbf{r}', t)$ may be achieved.

The imaging method employed here is that of Filtered Back Projection in which the time delay between radiofrequency (rf) excitation and signal acquisition is minimized, thus reducing relaxation effects. Fig. 2 a shows the combined sequence used in the present work in which two intense (G_z) gradient pulses are applied normal to the sample's transverse section with subsequent imaging gradients applied in the x–y plane, commencing at the echo center. Fig. 2 b shows a similar sequence in which selective rf pulse slice excitation is employed, a scheme more appropriate where noninvasive imaging is desired.
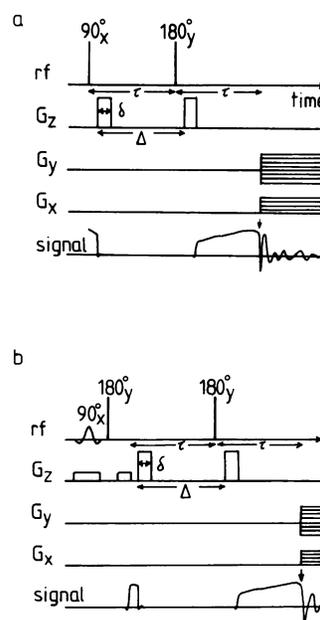
FIGURE 2 Two-dimensional Filtered Back Projection spin echo acquisition scheme employing a preceding pulsed gradient sequence to provide diffusion contrast in the image. The sequences illustrated in a and b correspond to nonselective and slice-selective excitation respectively.

In the filtered Back Projection (6) method the imaging field gradient magnitude G is fixed while G_x and G_y are adjusted. The image reconstruction consists of the two-dimensional Fourier Transformation,

$$\rho(x, y) = \int_0^\pi \int_{-\infty}^\infty S(k, \phi) \exp(-i2\pi \mathbf{k} \cdot \mathbf{r})|k|dkd\phi,$$

where $k = (2\pi)^{-1} \gamma |G| t$

$\phi = \tan^{-1}[G_x/G_y]$

and $\mathbf{k} \cdot \mathbf{r} = k(x \cos\phi + y \sin\phi).$ (5)

EXPERIMENTAL

The imaging system is based on a JEOL FX 60 NMR spectrometer. It includes a modified probe incorporating quadrupolar G_x and G_x gradient coils capable of producing 250 and 150 G cm^{-1} respectively with switching times of 20 μs. The G_y gradient uses a shim coil capable of 3 G cm^{-1}. Gradient and rf levels and switching logic are determined by a specially constructed pulse programmer under software control. Generation of experimental sequence parameters and subsequent data analysis is performed using an MB 16000 (8088 based) pc (Hitachi, Japan) which incorporates a high resolution color graphics monitor. Images are recorded as 16 bit 256 × 256 pixel arrays.

Wheat (*Triticum aestivum* L., cv. Otane) was grown in 10-liter containers of soil. Transverse sections 1.3 mm of wheat grains at the mid grain filling stage of development were obtained by slicing and were mounted between microscope cover slides 1.5-mm apart. These were then inserted in 5-mm NMR tubes in which moist cotton wool was incorporated a few millimeters above the sample in order to maintain atmospheric humidity. The grain water content was 53% by weight determined by weighing a companion grain. No significant water loss was observed over the several hours required to acquire the images with differing pulsed gradient magnitude. The samples were oriented with their transverse sections in the x-y plane.

It is noteworthy that gradients of order 100 G cm^{-1} are required to measure water diffusion if the spin echo timescale is to be compressed to a few milliseconds in order to avoid T_2 relaxation. In the wheat samples, T_2 values were typically 30 ms and the sequence used here employed $\tau = 5$ ms, $\delta = 2$ ms, and $\Delta = 5$ ms. The pulsed G_z gradient used is an order of magnitude larger than that reported to be available in other microscopic imaging systems (10, 11). G_z was calibrated to 1% by PGSE using the known diffusion coefficient of pure water, and by direct imaging of a water sample of known dimensions. The imaging gradient of 3 G cm^{-1} was stepped in orientation from 0° to 178° in 2° steps. 48 acquisitions were used per back projection with a sampling and filter bandwidth of 10 kHz. An exponential digital filter was applied in order to improve signal to noise and this limited the transverse resolution to 150 μm. All measurements were performed at 28 ± 1°C.

RESULTS AND DISCUSSION

Fig. 3 shows an image obtained at zero pulsed (G_z) gradient along with an intensity profile along a line in the image. The peak/rms signal to noise is ~ 110:1. Differing water intensities in the endosperm tissue and vascular bundle area are immediately apparent, broad features being identified in the legend to Fig. 3. The localized self-diffusion experiment was performed by varying G_z as shown in Fig. 4. A decay in water proton signal intensity is apparent as G_z is increased, and the rate of attenuation differs in the various structural features, indicating differing self-diffusion rates. By measuring the echo image signal strength $A(G_z)$ as a function of G_z at specified
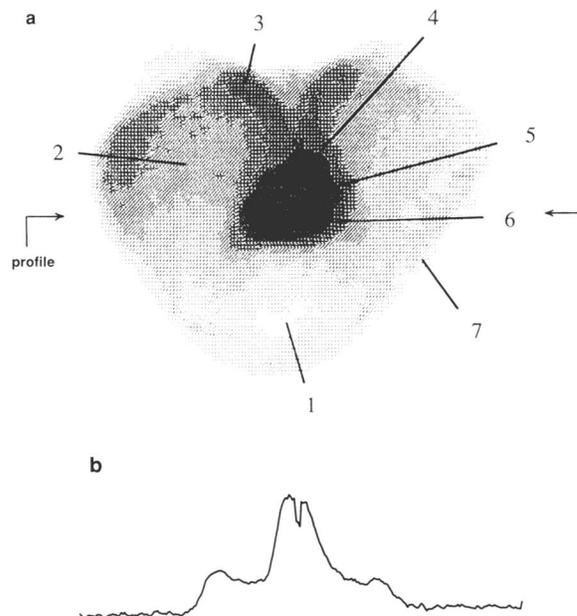
FIGURE 3 (*a*) Image of transverse section of a wheat grain indicating the location of its major structural features. The endosperm (regions 1, 2, and 3) is the organ in which starch is deposited; at this stage of development starch comprises ~ 80% of its dry weight. The outer layer of the endosperm (the aleurone layer) the seed coat (testa) and the wall of the fruit (pericarp) are not resolved and together correspond to region 7. Longitudinal transport of water and solutions of nutrients is provided by xylem and phloem vessels in vascular bundles scattered through region 4. Nutrients travel from the vascular bundles into the endosperm via the chalaza and nucellar projection (region 5) and through a liquid filled cavity occupying part of region 6. (*b*) Intensity profile taken along line indicated in *a*.
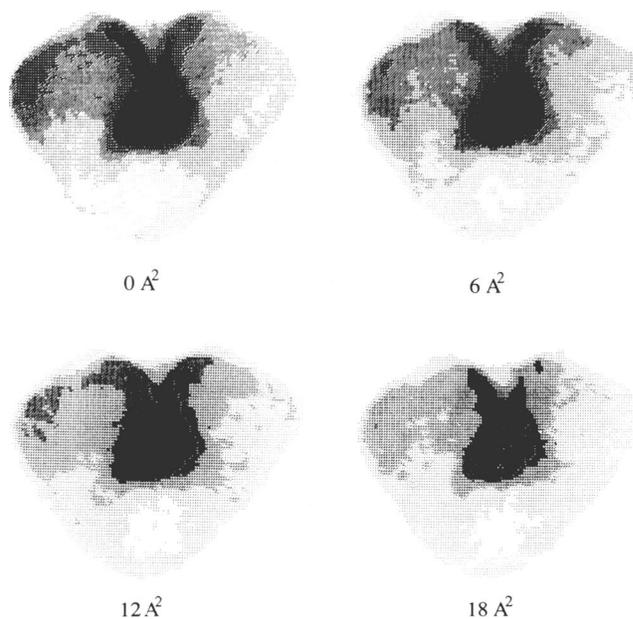
FIGURE 4 Illustration of the influence of the preceding pulsed gradient sequence as in Fig. 3. As the magnitude of these gradient pulses is increased, the spin echo image amplitude decreases at a rate determined by the local water-diffusion rate.
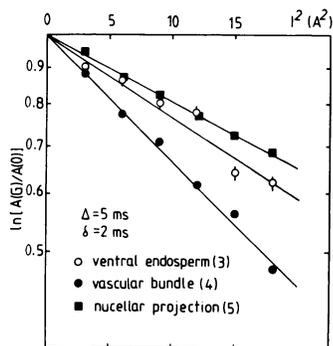
FIGURE 5 Spin echo attenuation plots from regions 3, 4, and 5 showing the exponential dependence of image amplitude of G_z^2 in accordance with Eq. 4. The self-diffusion coefficients obtained are given in TABLE I.

TABLE 1
LOCALIZED WATER SELF-DIFFUSION NORMAL TO TRANSVERSE SECTION OF WHEAT KERNEL

Region*	Identification	D
		$m^2 \, s^{-1}$
1	Dorsal endosperm	5 (3) $\times 10^{-10}$
2	Cheek endosperm	7.0 (5) $\times 10^{-10}$
3	Ventral endosperm	7 (1) $\times 10^{-10}$
4	Vascular bundle + chalaza	10.1 (5) $\times 10^{-10}$
5	Nucellar projection	5 (2) $\times 10^{-10}$
6	Endosperm cavity	10.6 (8) $\times 10^{-10}$
7	Aleurone layer + testa + pericarp	9 (3) $\times 10^{-10\ddagger}$

*See Fig. 3 a.

‡These data are subject to errors associated with defining a consistent region close to the image boundary.

locations, the normalized echo alternations are plotted as in $(A[G_z]/A[0])$ vs. G_z^2 and yield linear dependences as described by the Stejskal-Tanner relationship, in Eq. 4. Echo attenuation plots are shown in Fig. 5 and the water self-diffusion coefficients obtained are summarized in Table I. The results indicate significant reductions below the free water value of 2.3×10^{-9} m^2s^{-1} at 28°C and are consistent with the bulk averages obtained in the previous studies.

Motion of water is most severely hindered in the endosperm; some, but probably not all of the reduction in diffusion can be explained by the high content of starch (Jenner, C.F., and G.P. Jones, manuscript in preparation). Water appears less hindered in regions 4, 5, and 6, the route taken by nutrients moving into the endosperm. Comparative freedom of diffusion in the vicinity of the vascular bundles is consistent with recent ideas on the flow of water within this region of the grain (12).

All nutrients entering the grain flow as aqueous solution along the vascular bundle (region 4) in sieve tubes a few micrometers in diameter. Water and solutes are unloaded from the sieve tubes and although little is known about this process it is presumed to regulate the entry of solutes into the endosperm (13). Information on concentration of solute in the sieve tubes (13) and on the numbers and dimensions of the sieve tubes (14) is available. However investigation of the mechanisms of unloading requires also data on the velocity of flow along the sieve tubes and on the kinetics of the escape of solute and water from them. Meanwhile, the values reported here on the diffusion of water in the unloading region permit physiological studies on the kinetics of unloading by radioisotope analysis based on models described by, for example, Horwitz (15).

CONCLUSION

The present use of pulsed magnetic field gradients as an image contrast mechanism in NMR spin echo imaging reveals the capacity of NMR microscopy to reveal local dynamical features at high resolution. One specific advantage of NMR imaging is its molecular specific quality and in the present example, where the image is dominated by the water proton contribution, we have determined water

self-diffusion normal to the imaging plane. By use of appropriate selective excitation (16) it should be possible to measure the localized transport of the selected molecular species in any desired direction.

REFERENCES

1. Lauterbur, P. C. 1973. Image formation by induced local interactions: examples employing nuclear magnetic resonance. Nature (Lond.). 242:190–191.
2. Mansfield, P., and P. K. Grannel. 1973. NMR diffraction in solids? J. Phys. C. 6:L422–426.
3. Carr, H. Y., and E. M. Purcell. 1954. Effects of diffusion on free precession in nuclear magnetic resonance Experiments. Phys. Rev. 94:630–638.
4. Stejskal, E. O., and J. E. Tanner. 1965. Spin diffusion measurements: spin echoes in the presence of a time dependent field gradient. J. Chem. Phys. 42:288–292.
5. Eccles, C. D., and P. T. Callaghan. 1986. High-resolution imaging. The NMR microscope. J. Magn. Reson. 68:393–398.
6. Mansfield, P., and P. G. Morris. 1982. NMR imaging in biomedicine. In Advances in Magnetic Resonance. Suppl. 2. J. S. Waugh, editor. Academic Press, Inc., New York.
7. Callaghan, P. T., and C. D. Eccles. 1987. Sensitivity and resolution in NMR imaging. J. Magn. Reson. 71:426–445.
8. Callaghan, P. T., K. W. Jolley, and J. Lelievre. 1979. Diffusion of water in the endosperm tissue of wheat grains studied by pulsed field gradient nuclear magnetic resonance. Biophys. J. 28:133–142.
9. Callaghan, P. T. 1984. Pulsed field gradient nuclear magnetic resonance as a probe of liquid state molecular organisation. Aust. J. Phys. 37:359–387.
10. Aguayo, J. B., S. J. Blackband, J. Schoeniger, M. A. Mattingly, and M. Hinterman. 1986. Nuclear Magnetic resonance imaging of a single cell. Nature (Lond.). 322:190–191.
11. Hall, L. D., S. Luck, and V. Rajanayagam. 1986. Construction of a high-resolution NMR probe for imaging with submillimeter spatial resolution. J. Magn. Reson. 66:349–351.
12. Jenner, C. F. 1985. Transport of tritiated water and ¹⁴C-labelled

assimilate into grains of wheat III. Diffusion of THO through the stalk. *Aust. J. Plant Physiol.* 12:595–607.

13. Fisher, D. B., and R. M. Gifford. 1986. Accumulation and conversion of sugars by developing wheat grains. IV. Gradients along the transport pathway from the peduncle to the endosperm cavity during grain filling. *Plant Physiol. (Bethesda).* 82:1024–1030.

14. O'Brien, T. P., M. E. Sammut, J. W. Lee, and M. G. Smart. 1985. The vascular system of the wheat spikelet. *Aust. J. Plant Physiol.* 12:487–511.

15. Horwitz, L. 1958. Some simplified mathematical treatments of translocation in plants. *Plant Physiol. (Bethesda).* 33:81–93.

16. Axel, L., and L. Dougherty. 1986. Chemical-shift-selective magnetic resonance imaging of multiple line spectra by selective saturation. *J. Magn. Reson.* 66:194–196.